New Type of Stable Particlelike States in Chiral Magnets

Filipp N. Rybakov,[1] Aleksandr B. Borisov,[1] Stefan Blügel,[2] and Nikolai S. Kiselev[2,*]

[1]*M.N. Miheev Institute of Metal Physics of Ural Branch of Russian Academy of Sciences, Ekaterinburg 620990, Russia*
[2]*Peter Grünberg Institut and Institute for Advanced Simulation, Forschungszentrum Jülich and JARA, D-52425 Jülich, Germany*

We present a new type of thermodynamically stable magnetic state at interfaces and surfaces of chiral magnets. The state is a soliton solution of micromagnetic equations localized in all three dimensions near a boundary, and it contains a singularity but nevertheless has finite energy. Both features combine to form a quasiparticle state for which we expect unusual transport and dynamical properties. It exhibits high thermal stability and thereby can be considered as a promising object for fundamental research and practical applications in spintronic devices. We identified the range of existence of such particlelike states in the thickness dependent magnetic phase diagram for helimagnet films and analyzed its stability in comparison with the isolated skyrmion within the conical phase. We provide arguments that such a state can be found in different B20-type alloys, e.g., $Mn_{1-x}Fe_xGe$, $Mn_{1-x}Fe_xSi$, $Fe_{1-x}Co_xSi$.

Many branches of modern physics focus on systems that exhibit a rich variety of metastable states. Special attention is drawn to systems characterized by a high-energy barrier, which are able to persist in a particular metastable state for an unbounded or noticeably long time. Such systems are within the scope of interest for optical, magnetic, and electronic data storage technology. Basically, almost all modern electronics and spintronics are based on handling and manipulating such metastable states. For instance, the magnetic domains in magnetic data storage devices are the best examples of such metastable states separated by high-energy barriers. In hard disk drives, high-energy barriers are provided by a high magnetocrystalline anisotropy of the material, which, at the same time, makes the magnetic domains motionless and affixed to their positions. The disadvantage of such data storage is that the detector has to be moved to the place where the data bit is stored, or the whole storage media has to be moved towards the detector.

Modern spintronics offers many alternative ideas for the next-generation magnetic data storage devices that are based on utilizing movable metastable states. The most promising candidates are domain walls in nanowires [1] and localized magnetic vortices [2], also known as chiral magnetic skyrmions [3,4]. The latter appear in magnets with a Dzyaloshinskii-Moriya interaction (DMI) [5,6] as an isolated metastable state or as a ground state, when skyrmions condense into a lattice.

From the point of view of field theory, skyrmions are two-dimensional solitons known as an exception to the Hobart-Derrick theorem [7] because of the presence of Lifshitz invariants [8]. Because of their unusual transport properties, and compact size, which under some conditions can be reduced up to a few nanometers [9] or even a few atomic distances [10], such types of chiral vortices are considered as promising particles for information technology as well as an interesting subject for fundamental research in nonlinear physics.

In this Letter, we present a new type of metastable particlelike state—a hybrid particle composed of a smooth magnetization vector field and a magnetic singularity. It is a three-dimensionally localized soliton of the nonlinear equations for a unit vector field. Such a quasiparticle is more compact, and it turns out to be energetically more favorable than the chiral magnetic skyrmion in a wide range of parameters.

Our approach is based on a classical spin model of the simple cubic lattice described by the following Hamiltonian [11] consisting of three contributions: the Heisenberg exchange interaction, the Dzyaloshinskii-Moriya interaction, and the Zeeman term

$$E = -J\sum_{\langle ij \rangle} \mathbf{n}_i \cdot \mathbf{n}_j - \sum_{\langle ij \rangle} \mathbf{D}_{ij} \cdot [\mathbf{n}_i \times \mathbf{n}_j] - \mu_s \mathbf{H}\sum_i \mathbf{n}_i, \quad (1)$$

where $\langle ij \rangle$ denote summation over all nearest-neighbor pairs, $\mathbf{n}_i = \mathbf{M}_i/\mu_s$ is a unit vector of the magnetic moment at lattice site i, J is the exchange coupling constant, and $\mathbf{D}_{ij}$ is the Dzyaloshinskii-Moriya vector defined as $\mathbf{D}_{ij} = D\mathbf{r}_{ij}$, D is the DMI scalar constant, $\mathbf{r}_{ij}$ is a unit vector pointing from site i to site j, and $\mathbf{H}$ is an external magnetic field applied along the z axis, perpendicular to the film plane. Note, we assume isotropic DMI, which means that the value $|\mathbf{D}_{ij}|$ is fixed for all three spatial directions. A periodic boundary condition is applied in the xy plane.

In order to preserve the generality of the results of our discrete model and to be able to compare them to the earlier developed theory based on continuum approximation [2,12–15], we use the following notations:

$$L_D = 4\pi\frac{\mathcal{A}}{\mathcal{D}} = 2\pi a\frac{J}{D}, \quad H_D = \frac{\mathcal{D}^2}{2M_s\mathcal{A}} = \frac{D^2}{\mu_s J}, \quad (2)$$

where L_D is the lowest period of the incommensurate spin spiral which exists below the critical field H_D, $\mathcal{A}$ and $\mathcal{D}$ are micromagnetic constants of exchange and DMI, respectively, M_s is the magnetization of the material, and a is the lattice constant.

We use a nonlinear conjugate gradient method with adaptive stereographic projections implemented on NVIDIA CUDA architecture for direct minimization of the Hamiltonian (1) [16].

In order to identify the range of parameters corresponding to the stable configurations, we have calculated the magnetic phase diagram for the ground state (see Fig. 1). Here, solid lines correspond to the first-order phase transition between the helical state [17], skyrmion lattice (SkL), conical phase, and saturated state. The horizontal dashed line between conical and saturated states corresponds to the second-order phase transition. Under the condition where L_D is 1 order of magnitude or more larger than a, discrete (1) and continuum [16] approaches are consistent.

Results presented in Fig. 1 are consistent with the continuum theory [18] and experimental data on the direct observation of SkL in thin films of cubic helimagnetic alloys such as $Fe_{1-x}Co_xSi$ [11], $Mn_{1-x}Fe_xGe$ [9], $Mn_{1-x}Fe_xSi$ [19], and pure MnSi [20] and FeGe [21]. The mechanism of SkL stabilization in thin films of a cubic helimagnet differs from two-dimensional systems with interface-induced DMI [22] and anisotropic bulk helimagnets [23,24]. According to Ref. [18], the free boundary of the layer that provides an additional degree of freedom to the magnetic system and changes the common energy balance is responsible for the SkL stabilization. In particular, because of the lack of exchange coupled neighbors on
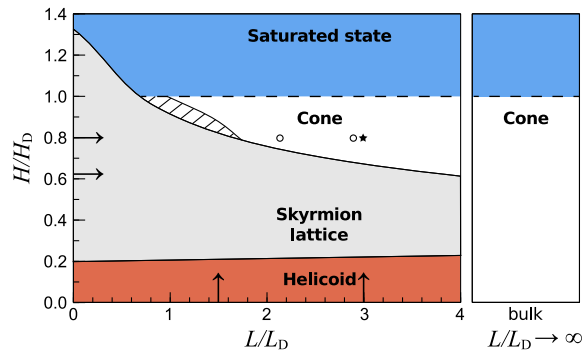
the surface, the spin structure of an isolated skyrmion tube (SkT) exhibits a small twist of magnetization with respect to the surface normal, as schematically shown in Fig. 2(a). Such an induced twist propagates through the whole thickness of the sample, accumulates the energy gain of the DMI contribution along the z axis, and results in significant reduction of the total energy of the SkT. As a result, within a certain range of applied field, the energy of the SkL becomes lower than the energy of the conical phase. The equilibrium value of the angle for such a surface twist is defined by the competition between positive contributions of exchange coupling and two negative contributions: (i) in-plane DMI between the spins in the same plane and (ii) out-of-plane DMI between the spins along the z axis. For the SkT and ChB, this angle $\varphi_0 \lesssim 15°$ (see Fig. 2). Recently, the effect of the chiral surface twist has been proven experimentally [25,26].

Everywhere within the conical phase, the lowest-energy metastable state corresponds to that shown in Fig. 2(b). The exception is the small dashed area in Fig. 1 where SkT dominates.

The vector field corresponding to such a solution is characterized by the shape of the isosurface $n_z = 0$, which is close to the shape of a paraboloid (Fig. 2(b)). An essential element of the corresponding magnetic structure is a singularity situated at a finite distance P from the surface (see the green sphere at the bottom of the red isosurface). This type of singularity is known in ferromagnets as the Bloch point (BP) or hedgehog [27], and in other condensed matter systems, e.g., ultracold gas [28] and spin ice [29], as a magnetic monopole. In helimagnets, because of the

FIG. 1 (color online). Phase diagram of the ground state for isotropic helimagnetic thin film of thickness L at magnetic field H applied normally. The dashed area within the conical ground state corresponds to the isolated skyrmion as the lowest-energy metastable state. Arrows indicate the values of the fixed parameters used in the energy calculation presented in Figs. 3(a)–3(d). The star symbol corresponds to the parameters used for the calculation of the nonzero anisotropy case [see Figs. 3(e) and 3(f)]; the circles are for the calculation of the energy barriers (see Fig. 4).
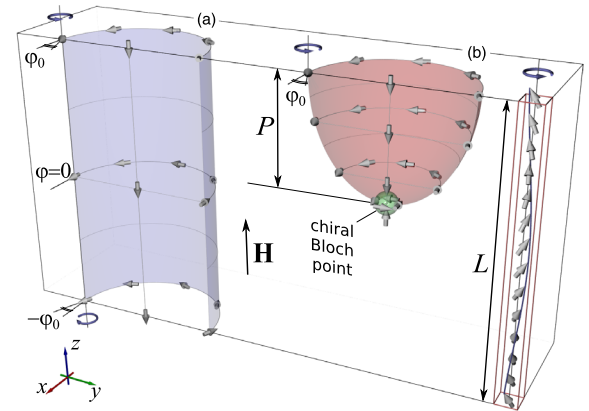

FIG. 2 (color online). Schematic representation of the vector field and cross sections of corresponding isosurfaces ($n_z = 0$) for the SkT (a) and chiral bobber (ChB) (b). The small (green) sphere indicates the position of the chiral Bloch point. The spins in red-outlined box on the right illustrate the magnetization distribution in the conical phase, which surrounds these localized metastable states. Circular blue arrows indicate the sense of magnetization rotation within the conical phase and surface-induced twist. For the exact spin structure of SkT and ChB see Ref. [16] (Movies 1 and 2).

presence of DMI, the vector field around the singularity exhibits a chiral structure. Thus, we refer to it as the chiral BP. Earlier, it was shown that some dynamical processes in chiral magnets are accompanied by the appearance of this kind of singularity [30,31]. We succeeded to get an analytical expression for the vector field in close vicinity to the chiral BP, which gives an opportunity to estimate its energy contribution to the total energy of the system [16].

In the cross section with the plane parallel to the layer surface, its spin structure mimics the magnetization distribution of the skyrmion with the diameter diminishing with distance from the surface. We found that the value of the penetration depth always satisfies the condition $P \leq L_D/2$ with an accuracy up to $\pm a/2$. Because of the essential chirality of such a state and its localization close to the surface with the finite penetration depth, like a fishing bobber on the water's surface, we use the term chiral bobber (ChB) to refer to this object.

We calculated the energy dependence of the ChB and SkT at the applied field and varying thickness [see Figs. 3(a)–3(d)]. Here, we use the same color notation as in the phase diagram, Fig. 1: White and grey areas correspond

to the stability range of the conical phase and SkL, respectively, and the dashed area denotes the range within the conical ground state where the SkT is lower in energy than the ChB. As follows from Figs. 3(a)–3(d), almost everywhere within the conical phase, the ChB has energy much lower than the SkT. The energy difference between the ChB and SkT becomes most pronounced by varying the thicknesses [see Figs. 3(c) and 3(d)]. The energy of the SkT increases linearly with the thickness. At the same time, because of the localization of the ChB near the surface, its energy is almost independent of thickness. It shows significant variation only at low fields and very small thicknesses, outside of the range of the conical phase stability [see insets in Fig. 3(d)].

In order to estimate the stability of the ChB in anisotropic systems, we add to the model Hamiltonian, Eq. (1), the following term:

$$E_K = -\sum_i \{K_u n_{i,z}^2 + K_c[n_{i,x}^4 + n_{i,y}^4 + n_{i,z}^4]\}, \quad (3)$$

where $n_{i,x}$ is the x component of unity vector **n** at the lattice site i, K_c is the cubic anisotropy constant, and K_u is the
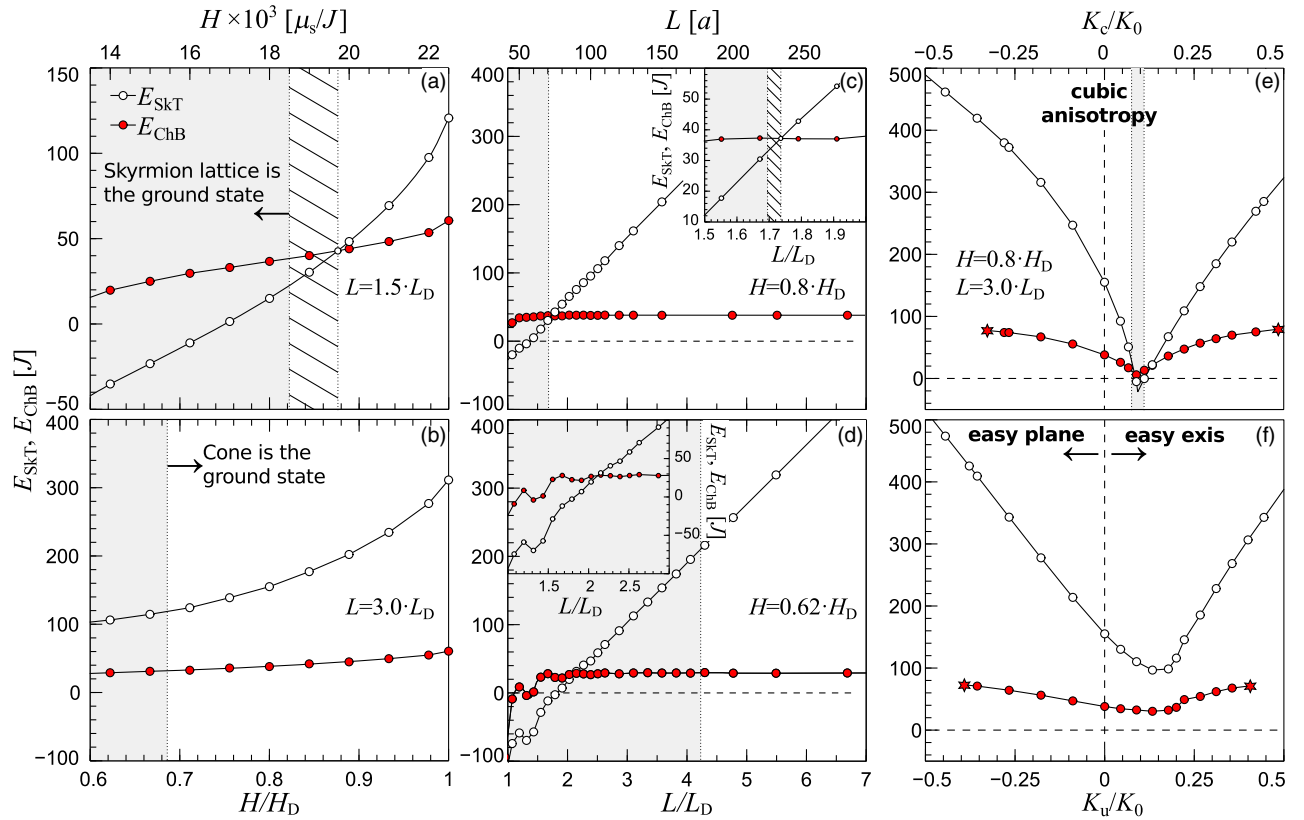

FIG. 3 (color online).   Energy dependence for isolated SkT (open circles) and ChB (red solid circles) on the applied magnetic field for fixed film thickness (a,b), on film thickness for the fixed applied field (c,d), and as a function of varying values of cubic (e) and uniaxial anisotropy (f) for fixed thickness and field. The energies are presented relative to the pure conical phase. Note, the cases in (a)-(d) correspond to the isotropic case, $K_c = K_u = 0$. The top and bottom scales in (a,b) and (c,d) are identical but given in absolute and reduced units, respectively. For these calculations, we used $J = 1$, $D = 0.15$ ($L_D = 41.89a$) and a size of the simulated domain of $256 \times 256 \times L_n$ spins, where $L_n = 40 \div 280$.

constant of uniaxial anisotropy induced in the system, e.g., by the interfaces or under external stress. In Figs. 3(e) and 3(f), the energies of the ChB and SkT are presented as functions of varying anisotropy constants at the fixed applied field $H = 0.8H_D$ and thickness $L = 3L_D$. We use reduced units of anisotropy where $K_0 = a^3 \mathcal{D}^2/(4\mathcal{A}) = D^2/(2J)$.

As follows from the figures, in the whole range of existence within the conical phase, the ChB remains energetically more favorable than the SkT. The star symbols in Figs. 3(e) and 3(f) correspond to the collapse of the ChB. In Fig. 3(e), the narrow gray region denotes the range of SkL stability, which is consistent with previous theoretical studies [24].

Because of the presence of free boundaries and singularities as an essential element of the solution, the topology of such an object should be described in the frame of relative homotopy groups [32]. Since our boundary conditions impose no restrictions on the magnetization, as an order parameter, the corresponding group is trivial, $\pi_2(\mathbb{S}^2, \mathbb{S}^2) = 0$. This means that the singularity can be pushed out on the surface and then smoothed. It is important to emphasize that when certain restrictions to the order parameter are imposed at the boundary, this may lead to formation of topologically nontrivial states, as in the case of a boojum in the A phase in ^{3}He [33,34]. Despite the fact that the solution for the ChB is nontopological, it shows the high-energy barrier.

In order to estimate the energy barriers, we have calculated the minimum energy path (MEP) with the geodesic nudged elastic band (GNEB) method [35], which is an extension of the original nudged elastic band method [36,37] to magnetic systems. In the GNEB method, the curvature of the configuration space of a magnetic system arising from a constraint on the length of magnetic moments is taken into account. The path between the metastable states is presented by the discrete sequence of system snapshots called images. These images are then brought to the MEP in the curved configuration space.

Examples of MEPs are presented in Fig. 4. For these calculations, we used the following parameters: $J = 1$, $D = 0.45$ ($L_D = 13.96a$) and a domain size of $30 \times 30 \times 30$ and $30 \times 30 \times 40$. The elimination of the SkT occurs via nucleation of a pair of chiral BPs (point b) moving towards opposite surfaces, and it results in the appearance of two repulsive ChBs (point c) which have energy higher than two isolated ChBs.

As follows from Fig. 4, the energy barriers for the ChB and the SkT have comparable height, $\Delta E_{ef} = 0.43\Delta E_{ab}$ for L_1 and $\Delta E_{ef} = 0.28\Delta E_{ab}$ for L_2. From this, we may conclude that the thermal stability range for ChB is expected to be of the same order of magnitude as for isolated SkT. Moreover, because of the high activation energy required for the SkT nucleation and complexity of the MEP, we may expect that the probability of
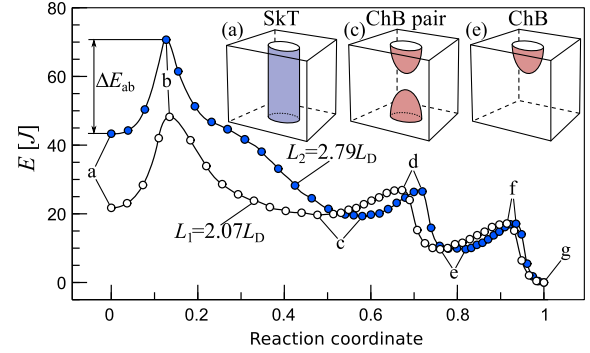

FIG. 4 (color online). Minimum energy path calculated for $L_1 = 2.07L_D$, and $L_2 = 2.79L_D$ at $H/H_D = 0.8$, $K_c = K_u = 0$. The reaction coordinate is an order parameter that represents the relative distance between the states in the configuration space [35]. The local minima a, c, and e correspond to the energies of SkT, a pair of ChBs, and a single ChB, respectively (see, also, the schematic representation in the corresponding insets). The difference between the energy values in the local minimum and nearest maximum corresponding to the saddle points (see b, d, and f) defines the energy barrier responsible for the stability of the corresponding state. The reference level ($E = 0$) is the energy of the global minimum g corresponding to the pure conical phase [16].

spontaneous nucleation of the skyrmions driven by thermal fluctuation, at least in this regime, has to be much lower in comparison to the ChB. Indeed, $\Delta E_{gb} = 2.8\Delta E_{gf}$ for L_1, and $\Delta E_{gb} = 4.1\Delta E_{gf}$ for L_2. This simple argument is confirmed by the results of our Monte Carlo simulation. In particular, for the parameters $L = 2.36L_D$ and $H = 0.8H_D$, the spontaneous nucleation of the ChBs has been observed during the simulated annealing, while the spontaneous nucleation of the SkT has not been observed in this regime at all [16].

In conclusion, we have shown that for isotropic and weakly anisotropic helimagnets, the chiral bobber corresponds to the lowest-energy metastable state in a wide range of thicknesses and applied fields. It exhibits high thermal stability, which supports our prediction to observe such a state at the surface of bulk chiral magnets, in thin films, or heterostructures of chiral magnets for thicknesses $L \geq 0.6L_D$. The most promising candidate material offering a direct observation of chiral bobbers seems to be $Mn_{1-x}Fe_xGe$, where the period of the spin spiral L_D can be controlled in a wide range (3–160 nm) by varying the concentration x of Fe [9]. Because of the three-dimensional nature of the object, off-axis electron holography in a transmission electron microscope is a promising technique visualizing its three-dimensional magnetic structure [38,39].

The chiral bobber constitutes a new class of particles— the hybrid particles composed of a smooth magnetization field and a magnetic singularity. Both contribute to three-dimensional torque fields and interesting dynamical and electron transport properties.

We speculate that the chiral Bloch point contributes to a nonzero scalar chirality that produces an orbital moment that can couple to optics. This new type of particle may offer the opportunity to introducing atomic-scale singularities as a new concept in spintronic device design.

---

*n.kiselev@fz-juelich.de

[1] S. Parkin and S-H. Yang, Nat. Nanotechnol. **10**, 195 (2015).
[2] A. N. Bogdanov and D. A. Yablonskii, Sov. Phys. JETP **68**, 101 (1989).[Zh. Eksp. Teor. Fiz. **95**, 178 (1989)].
[3] N. S. Kiselev, A. N. Bogdanov, R. Schäfer, and U. K. Rößler, J. Phys. D **44**, 392001 (2011).
[4] A. Fert, V. Cros, and J. Sampaio, Nat. Nanotechnol. **8**, 152 (2013).
[5] I. Dzyaloshinskii, J. Phys. Chem. Solids **4**, 241 (1958).
[6] T. Moriya, Phys. Rev. **120**, 91 (1960).
[7] R. Rajaraman, *Solitons and Instantons: An Introduction to Solitons and Instantons in Quantum Field Theory* (North-Holland, Amsterdam, 1982).
[8] A. Bogdanov, JETP Lett. **62**, 247 (1995).
[9] K. Shibata, X. Z. Yu, T. Hara, D. Morikawa, N. Kanazawa, K. Kimoto, S. Ishiwata, Y. Matsui, and Y. Tokura, Nat. Nanotechnol. **8**, 723 (2013).
[10] N. Romming, M. Menzel, C. Hanneken, J. E. Bickel, B. Wolter, K. von Bergmann, A. Kubetzka, and R. Wiesendanger, Science **341**, 636 (2013).
[11] X. Z. Yu, Y. Onose, N. Kanazawa, J. H. Park, J. H. Han, Y. Matsui, N. Nagaosa, and Y. Tokura, Nature (London) **465**, 901 (2010).
[12] A. Bogdanov and A. Hubert, J. Magn. Magn. Mater. **138**, 255 (1994).
[13] A. Bogdanov and A. Hubert, J. Magn. Magn. Mater. **195**, 182 (1999).
[14] U. K. Rößler, A. N. Bogdanov, and C. Pfleiderer, Nature (London) **442**, 797 (2006).
[15] U. K. Rößler, A. A. Leonov, and A. N. Bogdanov, J. Phys. Conf. Ser. **303**, 012105 (2011).
[16] See Supplemental Material at http://link.aps.org/supplemental/10.1103/PhysRevLett.115.117201 for details of micromagnetic analysis of the solutions, details of Monte Carlo simulations, exact spin structure corresponding to the skyrmion tube (Movie 1) and chiral bobber (Movie 2), and visualization of Monte Carlo simulation for thermally activated nucleation of the chiral bobber (Movie 3).
[17] I. E. Dzyaloshinskii, Sov. Phys. JETP **20**, 665 (1965).

[18] F. N. Rybakov, A. B. Borisov, and A. N. Bogdanov, Phys. Rev. B **87**, 094424 (2013).
[19] T. Yokouchi, N. Kanazawa, A. Tsukazaki, Y. Kozuka, M. Kawasaki, M. Ichikawa, F. Kagawa, and Y. Tokura, Phys. Rev. B **89**, 064416 (2014).
[20] X. Yu, A. Kikkawa, D. Morikawa, K. Shibata, Y. Tokunaga, Y. Taguchi, and Y. Tokura, Phys. Rev. B **91**, 054411 (2015).
[21] X. Z. Yu, N. Kanazawa, Y. Onose, K. Kimoto, W. Z. Zhang, S. Ishiwata, Y. Matsui, and Y. Tokura, Nat. Mater. **10**, 106 (2011).
[22] B. Dupe, M. Hoffmann, C. Paillard, and S. Heinze, Nat. Commun. **5**, 4030 (2014).
[23] M. N. Wilson, A. B. Butenko, A. N. Bogdanov, and T. L. Monchesky, Phys. Rev. B **89**, 094411 (2014).
[24] A. A. Leonov, Ph.D. thesis, Technical University Dresden (2012).
[25] M. N. Wilson, E. A. Karhu, D. P. Lake, A. S. Quigley, S. Meynell, A. N. Bogdanov, H. Fritzsche, U. K. Rößler, and T. L. Monchesky, Phys. Rev. B **88**, 214420 (2013).
[26] S. A. Meynell, M. N. Wilson, H. Fritzsche, A. N. Bogdanov, and T. L. Monchesky, Phys. Rev. B **90**, 014406 (2014).
[27] A. P. Malozemoff and J. C. Slonczewski, *Magnetic Domain Walls in Bubble Materials* (Academic Press, New York, 1979).
[28] M. W. Ray, E. Ruokokoski, S. Kandel, M. Möttönen, and D. S. Hall, Nature (London) **505**, 657 (2014).
[29] C. Castelnovo, R. Moessner, and S. L. Sondhi, Nature (London) **451**, 42 (2008).
[30] P. Milde, D. Köhler, J. Seidel, L. Eng, A. Bauer, A. Chacon, J. Kindervater, S. Mühlbauer, C. Pfleiderer, S. Buhrandt, C. Schütte, and A. Rosch, Science **340**, 1076 (2013).
[31] C. Schütte and A. Rosch, Phys. Rev. B **90**, 174432 (2014).
[32] G. E. Volovik, Sov. Phys. JETP Lett. **28**, 59 (1979).
[33] M. Monastyrsky, *Topology of Gauge Fields and Condensed Matter* (Springer, New York, 1993).
[34] G. E. Volovik, *The Universe in a Helium Droplet* (Oxford University Press, New York, 2003).
[35] P. F. Bessarab, V. M. Uzdin, and H. Jónsson, Comput. Phys. Commun. (2015).
[36] H. Jónsson, G. Mills, and K. W. Jacobsen, Nudged Elastic Band Method for Finding Minimum Energy Paths of Transitions, in *Classical and Quantum Dynamics in Condensed Phase Simulations*, edited by B. J. Berne, G. Ciccotti, and D. F. Coker (World Scientific, Singapore, 1998), p. 385.
[37] G. Henkelman and H. Jónsson, J. Chem. Phys. **113**, 9978 (2000).
[38] H. S. Park, X. Yu, S. Aizawa, T. Tanigaki, T. Akashi, Y. Takahashi, T. Matsuda, N. Kanazawa, Y. Onose, D. Shindo, A.Tonomura, and Y. Tokura, Nat. Nanotechnol. **9**, 337 (2014).
[39] P. A. Midgley and R. E. Dunin-Borkowski, Nat. Mater. **8**, 271 (2009).